

1                                   **A STABLE HIGH-ORDER PERTURBATION OF**  
2                                   **SURFACES/ASYMPTOTIC WAVEFORM EVALUATION METHOD**  
3                                   **FOR THE NUMERICAL SOLUTION OF GRATING SCATTERING**  
4                                   **PROBLEMS** \*

5                                   MATTHEW KEHOE   AND DAVID P. NICHOLLS †

6                   **Abstract.** The scattering of electromagnetic radiation by a layered periodic diffraction grating  
7 is an important model in engineering and the sciences. The numerical simulation of this experiment  
8 has been widely explored in the literature and we advocate for a novel interfacial method which is  
9 perturbative in nature. More specifically, we extend a recently developed High-Order Perturbation of  
10 Surfaces/Asymptotic Waveform Evaluation (HOPS/AWE) algorithm to utilize a stabilized numerical  
11 scheme which also suggests a rigorous convergence result. An implementation of this algorithm is  
12 described, validated, and utilized in a sequence of challenging and physically relevant numerical  
13 experiments.

14                   **Key words.** High-Order Perturbation of Surfaces Methods; Asymptotic Waveform Evaluation;  
15 High-Order Spectral Methods; Helmholtz equation; Layered Media.

16                   **AMS subject classifications.** 65N35, 78A45, 78B22

17                   **1. Introduction.** The scattering of linear waves by a periodic layered structure  
18 is a central model in many problems of scientific and engineering interest. Examples  
19 arise in areas such as geophysics [58, 5], imaging [38], materials science [24], nanoplas-  
20 monics [52, 35, 23], and oceanography [7]. In the particular case of nanoplasmonics,  
21 there are many important topics such as extraordinary optical transmission [22], sur-  
22 face enhanced spectroscopy [36], and surface plasmon resonance (SPR) biosensing  
23 [27, 37, 28, 31].

24                   Due to their technological importance, the numerical simulation of these diffrac-  
25 tion gratings has generated a huge amount of interest including the application of all  
26 of the classical approaches, e.g., Finite Differences [33], Finite Elements [29], Discon-  
27 tinuous Galerkin [26], Spectral Elements [21], and Spectral Methods [25, 6, 56]. For  
28 general geometries these specify extremely useful and accurate tools (e.g., COMSOL  
29 Multiphysics [18]) for engineers and scientists alike. However, for structures with  
30 simplifying features, such as homogeneous layering, these can be needlessly expensive  
31 due to the unnecessary discretization of layer interiors. To address this, a whole class  
32 of *interfacial* methods have been developed of which Boundary Integral/Boundary  
33 Element Methods (BIM/BEM) are the most widely used [17, 32, 55]. These posit  
34 unknowns at the layer interfaces thereby reducing the number of degrees of freedom  
35 by an order of magnitude. While these schemes require particular care in their imple-  
36 mentation (e.g., the design of special quadrature rules to achieve high-order accuracy,  
37 sophisticated algorithms to rapidly sum the quasi-periodized Green function, and ap-  
38 propriate preconditioning strategies for the iterative solution of the Non-Symmetric  
39 Positive Definite linear system of equations) there are well-known implementations  
40 that deliver results of surpassing accuracy and stability, see, e.g., [9, 10, 11].

41                   In this paper we focus upon a very particular Quantity of Interest (QoI) in the  
42 study of diffraction gratings, the Reflectivity Map, which is representative of a class

---

\*  
**Funding:** D.P.N. gratefully acknowledges support from the National Science Foundation through Grants No. DMS-1813033 and DMS-2111283.

†Department of Mathematics, Statistics, and Computer Science, University of Illinois at Chicago, Chicago, IL 60607 ([mkehoe5@uic.edu](mailto:mkehoe5@uic.edu), [davidn@uic.edu](mailto:davidn@uic.edu))

of performance metrics for which we develop a special class of interfacial numerical algorithms. The Reflectivity Map,  $R$ , measures the response (reflected energy) of a periodically corrugated grating structure as a function of illumination frequency,  $\omega$ , and corrugation amplitude,  $h$ . For each of the algorithms listed above, the response at any given  $(\omega, h)$  pair requires a new simulation restarted from scratch. A High-Order Perturbation of Surfaces (HOPS) method [46, 47] takes a perturbative view towards the geometric dependence of  $R$  on  $h = \varepsilon$ ,  $\varepsilon \ll 1$ , by seeking the terms in the expansion about  $\varepsilon = 0$ ,

$$R = R(\varepsilon) = \sum_{n=0}^{\infty} R_n \varepsilon^n.$$

With this one can realize an enormous savings in computational effort by conducting a new computation only for each choice of  $\omega$  and simply summing the formula above for any desired value of  $\varepsilon$ . We point out that the smallness requirement on  $\varepsilon$  can probably be dropped provided that  $\varepsilon$  is chosen to be *real* (see [45] for one possible strategy for establishing this result rigorously).

Taking this philosophy to its natural conclusion, in [40] we considered  $\omega = (1 + \delta)\underline{\omega} = \underline{\omega} + \delta\underline{\omega}$  and performed a *joint* expansion of this map about  $(\varepsilon = 0, \omega = \underline{\omega})$

$$R = R(\varepsilon, \delta) = \sum_{n=0}^{\infty} \sum_{m=0}^{\infty} R_{n,m} \varepsilon^n \delta^m.$$

It seems that a *single* computation, recovering all of the  $R_{n,m}$ , should be sufficient to discover the *entire* Reflectivity Map. In fact the situation is not so simple as these expansions are not valid for all values of  $(\varepsilon, \delta)$  and it was found in [40] that the Rayleigh singularities (often called the Wood anomalies) enforced finite-size domains of convergence in  $\delta$ . However, the results were so encouraging that we now undertake a more in-depth investigation featuring a new formulation in terms of Dirichlet-Neumann Operators computed via an application of the stable, accurate, and rapid Transformed Field Expansions (TFE) algorithm [47] appropriate for a *joint* perturbation expansion. Not only does this deliver an implementation with greatly enhanced stability properties [47], but it also describes an algorithm that can be rigorously justified to be convergent as we demonstrate in a forthcoming publication.

The paper is organized as follows. In Section 2 we summarize the equations which govern the propagation of linear electromagnetic waves in a two-dimensional periodic structure. In Section 2.1 we discuss the Transparent Boundary Conditions we utilize to enforce the outgoing wave conditions rigorously, while in Section 2.2 we define the object of our study, the Reflectivity Map. In Section 3 we restate our governing equations in terms of interfacial quantities via a Non-Overlapping Domain Decomposition phrased in terms of Dirichlet-Neumann Operators (DNOs). We discuss our HOPS/AWE approach in Section 4 and our novel approach to computing the DNOs in Section 5 (supplemented with a discussion of expansions of the surface data in Section 5.1). In Section 6 we present our numerical results with a description of implementation details in Section 6.1, our Fourier-Chebyshev method in Section 6.2, and our use of Padé approximation in Section 6.3. We comment on issues of the bounded domains of analyticity in our expansions in Section 6.4. In Section 6.5 we validate our code with the Method of Manufactured Solutions, while in Section 6.6 we present results of multiple numerical simulations of the Reflectivity Map which we conducted. In Section 6.7 we discuss the superior computational complexity our al-

87 gorithm enjoys for computing objects like the Reflectivity Map. Concluding remarks  
88 are given in Section 7.

89 **2. The Governing Equations.** In this paper we consider a  $y$ -invariant, doubly  
90 layered structure with a periodic interface separating the two materials; see Figure 1.  
The  $d$ -periodic interface shape is specified by the graph of the function  $z = g(x)$ ,

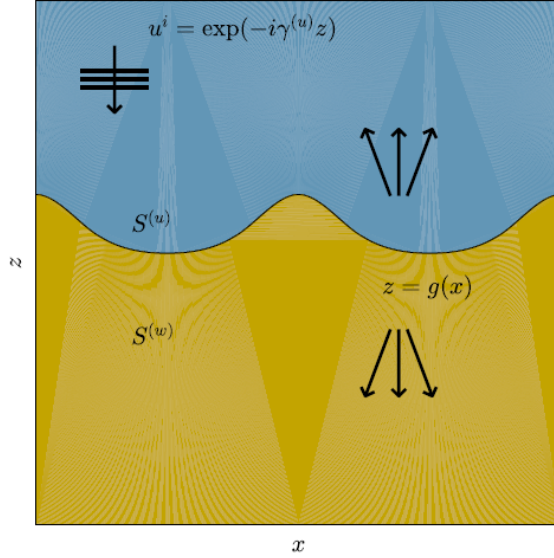


Fig. 1: A two-layer structure with a periodic interface,  $z = g(x)$ , separating two material layers,  $S^{(u)}$  and  $S^{(w)}$ , illuminated by plane-wave incidence.

91  $g(x + d) = g(x)$ . A dielectric (with refractive index  $n^u$ ) occupies the domain above  
92 the interface  
93

$$94 \quad S^{(u)} := \{z > g(x)\},$$

95 while a material of refractive index  $n^w$  is in the lower layer

$$96 \quad S^{(w)} := \{z < g(x)\}.$$

97 The superscripts are chosen to conform to the notation of the authors in previous  
98 work [39, 42]. The structure is illuminated from above by monochromatic plane-wave  
99 incident radiation of frequency  $\omega$  and wavenumber  $k^u = n^u\omega/c_0 = \omega/c^u$  ( $c_0$  is the  
100 speed of light) aligned with the grooves

$$101 \quad \underline{\mathbf{E}}^i(x, z, t) = \mathbf{A}e^{-i\omega t + i\alpha x - i\gamma^u z}, \quad \underline{\mathbf{H}}^i(x, z, t) = \mathbf{B}e^{-i\omega t + i\alpha x - i\gamma^u z},$$

$$102 \quad \alpha := k^u \sin(\theta), \quad \gamma^u := k^u \cos(\theta).$$

104 We consider the reduced incident fields

$$105 \quad \mathbf{E}^i(x, z) = e^{i\omega t} \underline{\mathbf{E}}^i(x, z, t), \quad \mathbf{H}^i(x, z) = e^{i\omega t} \underline{\mathbf{H}}^i(x, z, t),$$

106 where the time dependence  $\exp(-i\omega t)$  has been factored out. As shown in [49],  
 107 the reduced electric and magnetic fields  $\{\mathbf{E}, \mathbf{H}\}$  are  $\alpha$ -quasiperiodic like the incident  
 108 radiation. To close the problem we specify that the scattered radiation is “outgoing,”  
 109 upward propagating in  $S^{(u)}$  and downward propagating in  $S^{(w)}$ .

110 It is well known (see, e.g., Petit [49]) that in this two-dimensional setting, the  
 111 time-harmonic Maxwell equations decouple into two scalar Helmholtz problems which  
 112 govern the Transverse Electric (TE) and Transverse Magnetic (TM) polarizations.  
 113 We define the invariant ( $y$ ) direction of the scattered (electric or magnetic) field by  
 114  $\tilde{u} = \tilde{u}(x, z)$  and  $\tilde{w} = \tilde{w}(x, z)$  in  $S^{(u)}$  and  $S^{(w)}$ , respectively. The incident radiation in  
 115 the upper field is defined as  $\tilde{u}^i(x, z)$ .

116 Following our previous work [40] we further factor out the phase  $\exp(i\alpha x)$  from  
 117 the fields  $\tilde{u}$  and  $\tilde{w}$

$$118 \quad u(x, z) = e^{-i\alpha x} \tilde{u}(x, z), \quad w(x, z) = e^{-i\alpha x} \tilde{w}(x, z),$$

119 which, we note, are  $d$ -periodic. In light of all of this, we are led to seek outgoing,  
 120  $d$ -periodic solutions of

$$121 \quad (2.1a) \quad \Delta u + 2i\alpha \partial_x u + (\gamma^u)^2 u = 0, \quad z > g(x),$$

$$122 \quad (2.1b) \quad \Delta w + 2i\alpha \partial_x w + (\gamma^w)^2 w = 0, \quad z < g(x),$$

$$123 \quad (2.1c) \quad u - w = \zeta, \quad z = g(x),$$

$$124 \quad (2.1d) \quad \partial_N u - i\alpha(\partial_x g)u - \tau^2 [\partial_N w - i\alpha(\partial_x g)w] = \psi, \quad z = g(x),$$

126 where  $N := (-\partial_x g, 1)^T$ . The Dirichlet and Neumann data are

$$127 \quad (2.1e) \quad \zeta(x) := -e^{-i\gamma^u g(x)},$$

$$128 \quad (2.1f) \quad \psi(x) := (i\gamma^u + i\alpha(\partial_x g))e^{-i\gamma^u g(x)},$$

130 and

$$131 \quad \tau^2 = \begin{cases} 1, & \text{TE,} \\ (k^u/k^w)^2 = (n^u/n^w)^2, & \text{TM,} \end{cases}$$

132 where  $k^w = n^w \omega / c_0 = \omega / c^w$  and  $\gamma^w = k^w \cos(\theta)$ . Due to its importance in the  
 133 classical study of SPRs we will focus on TM polarization [52].

134 **2.1. Transparent Boundary Conditions.** The Upward Propagating Condi-  
 135 tion (UPC) and Downward Propagating Condition (DPC) [1] rigorously enforce the  
 136 outgoing wave conditions which we mentioned earlier. We now demonstrate how these  
 137 can be stated in terms of Transparent Boundary Conditions which also truncate the  
 138 bi-infinite problem domain to one of finite size. For this we choose values  $a$  and  $b$   
 139 such that

$$140 \quad a > |g|_\infty, \quad -b < -|g|_\infty,$$

141 and define the artificial boundaries  $\{z = a\}$  and  $\{z = -b\}$ . In  $\{z > a\}$  the Rayleigh  
 142 expansions [49] tell us that upward propagating solutions of (2.1a) are

$$143 \quad (2.2) \quad u(x, z) = \sum_{p=-\infty}^{\infty} \hat{a}_p e^{i\tilde{p}x + i\gamma_p^u z},$$

144 where, for  $q \in \{u, w\}$ ,

$$145 \quad (2.3) \quad \tilde{p} := \frac{2\pi p}{d}, \quad \alpha_p := \alpha + \tilde{p}, \quad \gamma_p^q := \sqrt{(k^q)^2 - \alpha_p^2}, \quad \text{Im} \{\gamma_p^q\} \geq 0.$$

146 In a similar fashion, downward propagating solutions of (2.1b) in  $\{z < -b\}$  can be  
147 expressed as

$$148 \quad w(x, z) = \sum_{p=-\infty}^{\infty} \hat{d}_p e^{i\tilde{p}x - i\gamma_p^w z}.$$

149 With these we can define the Transparent Boundary Conditions in the following way:  
150 Focusing on the UPC (the DPC is similar) we rewrite (2.2) as

$$151 \quad u(x, z) = \sum_{p=-\infty}^{\infty} \left( \hat{a}_p e^{i\gamma_p^u a} \right) e^{i\tilde{p}x + i\gamma_p^u (z-a)} = \sum_{p=-\infty}^{\infty} \hat{\xi}_p e^{i\tilde{p}x + i\gamma_p^u (z-a)},$$

152 and note that,

$$153 \quad u(x, a) = \sum_{p=-\infty}^{\infty} \hat{\xi}_p e^{i\tilde{p}x} =: \xi(x),$$

154 and

$$155 \quad \partial_z u(x, a) = \sum_{p=-\infty}^{\infty} (i\gamma_p^u) \hat{\xi}_p e^{i\tilde{p}x} =: T^u[\xi(x)],$$

156 which defines the order-one Fourier multiplier  $T^u$ . From this we state that upward-  
157 propagating solutions of (2.1a) satisfy the Transparent Boundary Condition at  $z = a$

$$158 \quad (2.4) \quad \partial_z u(x, a) - T^u[u(x, a)] = 0, \quad z = a.$$

159 We note that a similar calculation leads to the Transparent Boundary Condition at  
160  $z = -b$

$$161 \quad (2.5) \quad \partial_z w(x, -b) - T^w[w(x, -b)] = 0, \quad z = -b,$$

162 where

$$163 \quad T^w[\psi(x)] := \sum_{p=-\infty}^{\infty} (-i\gamma_p^w) \hat{\psi}_p e^{i\tilde{p}x}.$$

164 We also point out that solutions which satisfy (2.4) and (2.5) equivalently satisfy the  
165 UPC and DPC, respectively [1].

166 With these we now state the full set of governing equations as

167 (2.6a)  $\Delta u + 2i\alpha\partial_x u + (\gamma^u)^2 u = 0, \quad z > g(x),$

168 (2.6b)  $\Delta w + 2i\alpha\partial_x w + (\gamma^w)^2 w = 0, \quad z < g(x),$

169 (2.6c)  $u - w = \zeta, \quad z = g(x),$

170 (2.6d)  $\partial_N u - i\alpha(\partial_x g)u - \tau^2 [\partial_N w - i\alpha(\partial_x g)w] = \psi, \quad z = g(x),$

171 (2.6e)  $\partial_z u(x, a) - T^u[u(x, a)] = 0, \quad z = a,$

172 (2.6f)  $\partial_z w(x, -b) - T^w[w(x, -b)] = 0, \quad z = -b,$

173 (2.6g)  $u(x + d, z) = u(x, z),$

174 (2.6h)  $w(x + d, z) = w(x, z).$

176 **2.2. The Reflectivity Map.** Building upon the developments in the previous  
 177 section we can now define our QoI, the Reflectivity Map. Regarding the solution (2.2)  
 178 we note the very different character of the solution for wavenumbers  $p$  in the set

179 
$$\mathcal{U}^u := \{p \in \mathbf{Z} \mid \alpha_p^2 < (k^u)^2\},$$

180 and those that are not. From our choice of the branch of the square root, components  
 181 of  $u(x, z)$  corresponding to  $p \in \mathcal{U}^u$  propagate away from the layer interface, while those  
 182 not in this set decay exponentially from  $z = g(x)$ . The latter are called evanescent  
 183 waves while the former are propagating (defining the set of propagating modes  $\mathcal{U}^u$ )  
 184 and carry energy away from the grating. With this in mind one defines the efficiencies  
 185 [49]

186 
$$e_p^u := (\gamma_p^u / \gamma^u) |\hat{a}_p|^2, \quad p \in \mathcal{U}^u,$$

187 and the Reflectivity Map

188 (2.7) 
$$R := \sum_{p \in \mathcal{U}^u} e_p^u.$$

189 Similar quantities can be defined in the lower layer [49], and with these the principle  
 190 of conservation of energy can be stated for structures composed entirely of dielectrics

191 
$$\sum_{p \in \mathcal{U}^u} e_p^u + \tau^2 \sum_{p \in \mathcal{U}^w} e_p^w = 1.$$

192 In this situation a useful diagnostic of convergence for a numerical scheme (which we  
 193 will utilize later) is the “energy defect”

194 (2.8) 
$$D := 1 - \sum_{p \in \mathcal{U}^u} e_p^u - \tau^2 \sum_{p \in \mathcal{U}^w} e_p^w,$$

195 which should be zero for a purely dielectric structure.

196 **3. A Non-Overlapping Domain Decomposition Method.** We now restate  
 197 our governing equations (2.6) in terms of *surface* quantities via a Non-Overlapping  
 198 Domain Decomposition Method [34, 20, 19]. In particular, if we define

199 
$$U(x) := u(x, g(x)), \quad \tilde{U}(x) := -\partial_N u(x, g(x)),$$

200 
$$W(x) := w(x, g(x)), \quad \tilde{W}(x) := \partial_N w(x, g(x)),$$

202 where  $u$  is a  $d$ -periodic solution of (2.6a) and (2.6e), and  $w$  is a  $d$ -periodic solution of  
 203 (2.6b) and (2.6f). In terms of these our full governing equations (2.6) are equivalent  
 204 to the pair of boundary conditions, (2.6c) & (2.6d),

$$205 \quad U - W = \zeta, \quad -\tilde{U} - (i\alpha)(\partial_x g)U - \tau^2 \left[ \tilde{W} - (i\alpha)(\partial_x g)W \right] = \psi.$$

206 This set of two equations for four unknowns can be closed by noting that the pairs  
 207  $\{U, \tilde{U}\}$  and  $\{W, \tilde{W}\}$  are connected, e.g., by Dirichlet–Neumann Operators (DNOs)

$$208 \quad G : U \rightarrow \tilde{U}, \quad J : W \rightarrow \tilde{W}.$$

209 These are well-defined operators for sufficiently smooth  $g$  (e.g.,  $g \in C^2$  [47]) thus we  
 210 focus on this interfacial reformulation of our governing equations

$$211 \quad (3.1) \quad \mathbf{A}\mathbf{V} = \mathbf{R},$$

212 where

$$213 \quad (3.2) \quad \mathbf{A} = \begin{pmatrix} I & -I \\ G + (\partial_x g)(i\alpha) & \tau^2 J - \tau^2 (\partial_x g)(i\alpha) \end{pmatrix}, \quad \mathbf{V} = \begin{pmatrix} U \\ W \end{pmatrix}, \quad \mathbf{R} = \begin{pmatrix} \zeta \\ -\psi \end{pmatrix}.$$

214 **4. A High-Order Perturbation of Surfaces/Asymptotic Waveform Eval-**  
 215 **uation (HOPS/AWE).** At this point there are many approaches to simulate (3.1)  
 216 numerically. We take up a perturbative approach which makes two smallness assump-  
 217 tions:

- 218 1. Boundary Perturbation:  $g(x) = \varepsilon f(x)$ ,  $\varepsilon \in \mathbf{R}$ ,  $\varepsilon \ll 1$ ,
- 219 2. Frequency Perturbation:  $\omega = (1 + \delta)\underline{\omega} = \underline{\omega} + \delta\underline{\omega}$ ,  $\delta \in \mathbf{R}$ ,  $\delta \ll 1$ .

220 It is possible that one or both of these smallness demands can be relaxed, provided  
 221 that the parameters are real (c.f., [45, 48]). The second of these assumptions has the  
 222 following important consequences

$$223 \quad k^q = \omega/c^q = (1 + \delta)\underline{\omega}/c^q =: (1 + \delta)\underline{k}^q = \underline{k}^q + \delta\underline{k}^q, \quad q \in \{u, w\},$$

$$224 \quad \alpha = k^u \sin(\theta) = (1 + \delta)\underline{k}^u \sin(\theta) =: (1 + \delta)\underline{\alpha} = \underline{\alpha} + \delta\underline{\alpha},$$

$$225 \quad \gamma^q = k^q \cos(\theta) = (1 + \delta)\underline{\gamma}^q \cos(\theta) =: (1 + \delta)\underline{\gamma}^q = \underline{\gamma}^q + \delta\underline{\gamma}^q, \quad q \in \{u, w\}.$$

227 This, in turn, delivers

$$228 \quad \alpha_p = \alpha + \tilde{p} = \underline{\alpha} + \delta\underline{\alpha} + \tilde{p} =: \underline{\alpha}_p + \delta\underline{\alpha}.$$

229 At this point we now assume the *joint* analyticity of the operator  $\mathbf{A}$  and function  
 230  $\mathbf{R}$  with respect to  $\varepsilon$  and  $\delta$  which will induce a *jointly* analytic solution,  $\mathbf{V}$ , of (3.1).  
 231 (All of this will be rigorously established in a forthcoming publication.) In this case  
 232 we can expand

$$233 \quad (4.1) \quad \{\mathbf{A}, \mathbf{V}, \mathbf{R}\}(\varepsilon, \delta) = \sum_{n=0}^{\infty} \sum_{m=0}^{\infty} \{\mathbf{A}_{n,m}, \mathbf{V}_{n,m}, \mathbf{R}_{n,m}\} \varepsilon^n \delta^m,$$

234 and a straightforward calculation reveals that, at each perturbation order  $(n, m)$ , we  
 235 must solve

$$236 \quad \mathbf{A}_{0,0} \mathbf{V}_{n,m} = \mathbf{R}_{n,m} - \sum_{\ell=0}^{n-1} \mathbf{A}_{n-\ell,0} \mathbf{V}_{\ell,m} - \sum_{r=0}^{m-1} \mathbf{A}_{0,m-r} \mathbf{V}_{n,r}$$

$$237 \quad (4.2) \quad - \sum_{\ell=0}^{n-1} \sum_{r=0}^{m-1} \mathbf{A}_{n-\ell,m-r} \mathbf{V}_{\ell,r}.$$

238

239 At this point all that remains to be specified are the forms for the  $\mathbf{A}_{n,m}$  and  $\mathbf{R}_{n,m}$ ,  
 240 and a method to invert  $\mathbf{A}_{0,0}$ .

241 A brief inspection of the formulas for  $\mathbf{A}$  and  $\mathbf{R}$ , (3.2), reveals that

$$242 \quad (4.3a) \quad \mathbf{A}_{0,0} = \begin{pmatrix} I & -I \\ G_{0,0} & \tau^2 J_{0,0} \end{pmatrix},$$

$$243 \quad \mathbf{A}_{n,m} = \begin{pmatrix} 0 & 0 \\ G_{n,m} & \tau^2 J_{n,m} \end{pmatrix}$$

$$244 \quad (4.3b) \quad + \delta_{n,1} \{1 + \delta_{m,1}\} (\partial_x f)(i\alpha) \begin{pmatrix} 0 & 0 \\ 1 & -\tau^2 \end{pmatrix}, \quad n \neq 0 \text{ or } m \neq 0,$$

$$245 \quad (4.3c) \quad \mathbf{R}_{n,m} = \begin{pmatrix} \zeta_{n,m} \\ -\psi_{n,m} \end{pmatrix},$$

247 where  $\delta_{p,q}$  is the Kronecker delta function. The forms for  $\zeta_{n,m}$  and  $\psi_{n,m}$ , which depend  
 248 upon the incident radiation (e.g., we will investigate both a non-physical illumination  
 249 to validate our code, see Section 6.5, and plane-wave incidence, see Section 6.6), can  
 250 typically be stated explicitly. By contrast, formulas for the  $(n,m)$ -th corrections of  
 251 the Taylor expansions of the DNOs,  $G$  and  $J$ , must be simulated numerically. For  
 252 this we advocate the Method of Transformed Field Expansions (TFE) [47] which we  
 253 review in the following section.

254 **5. Simulation of Dirichlet–Neumann Operators.** As we mentioned in the  
 255 previous section, the only remaining specification for our algorithm is the computation  
 256 of the  $(n,m)$ -th term in the Taylor expansion of the DNOs,  $G$  and  $J$ . For brevity we  
 257 restrict our attention to the DNO in the upper layer,  $\{g(x) < z < a\}$ , and note that  
 258 the considerations for the lower layer are largely the same.

259 We recall the precise definition of the upper layer DNO [41]: Given an integer  
 260  $s \geq 0$  and any  $\theta > 0$ , if  $g \in C^{s+3/2+\theta}$  the unique  $d$ -periodic solution of

$$261 \quad (5.1a) \quad \Delta u + 2i\alpha \partial_x u + (\gamma^u)^2 u = 0, \quad g(x) < z < a,$$

$$262 \quad (5.1b) \quad u(x, g(x)) = U(x), \quad z = g(x),$$

$$263 \quad (5.1c) \quad \partial_z u(x, a) - T^u[u(x, a)] = 0, \quad z = a,$$

265 defines the Upper Layer Dirichlet–Neumann Operator

$$266 \quad (5.2) \quad G(g) : U \rightarrow \tilde{U} := -(\partial_N u)(x, g(x)).$$

267 To simulate the DNO numerically we appeal to the Method of Transformed Field  
 268 Expansions (TFE) [43, 47] which begins with a domain-flattening change of variables  
 269 (the  $\sigma$ -coordinates of oceanography [51] and the C-method of the dynamical theory  
 270 of gratings [16, 15])

$$271 \quad x' = x, \quad z' = a \left( \frac{z - g(x)}{a - g(x)} \right).$$

272 With this we can rewrite the DNO problem, (5.1), in terms of the transformed field

$$273 \quad u'(x', z') := u \left( x', \left( \frac{a - g(x')}{a} \right) z' + g(x') \right),$$



274 as (upon dropping primes)

$$275 \quad (5.3a) \quad \Delta u + 2i\alpha\partial_x u + (\gamma^u)^2 u = F(x, z), \quad 0 < z < a,$$

$$276 \quad (5.3b) \quad u(x, 0) = U(x), \quad z = 0,$$

$$277 \quad (5.3c) \quad \partial_z u(x, a) - T^u[u(x, a)] = J(x), \quad z = a,$$

278 and (5.2) as

$$280 \quad (5.4) \quad G(g)[U] = -\partial_z u(x, 0) + H(x).$$

281 The forms for  $\{F, J, H\}$  have been derived and reported in [47] and, for brevity, we  
282 do not repeat them here.

283 Following our HOPS/AWE philosophy we assume the joint boundary/frequency  
284 perturbation

$$285 \quad g(x) = \varepsilon f(x), \quad \omega = \underline{\omega} + \delta\underline{\omega},$$

286 and study the effect of this on (5.3) and (5.4). These become

$$287 \quad (5.5a) \quad \Delta u + 2i\underline{\alpha}\partial_x u + (\underline{\gamma}^u)^2 u = \tilde{F}(x, z), \quad 0 < z < a,$$

$$288 \quad (5.5b) \quad u(x, 0) = U(x), \quad z = 0,$$

$$289 \quad (5.5c) \quad \partial_z u(x, a) - T^u[u(x, a)] = \tilde{J}(x), \quad z = a,$$

291 and

$$292 \quad (5.6) \quad G(\varepsilon f)[U] = -\partial_z u(x, 0) + \tilde{H}(x).$$

293 In these

$$294 \quad \begin{aligned} \tilde{F} = & -\varepsilon \operatorname{div} [A_1(f)\nabla u] - \varepsilon^2 \operatorname{div} [A_2(f)\nabla u] - \varepsilon B_1(f)\nabla u - \varepsilon^2 B_2(f)\nabla u \\ 295 & - 2i\underline{\alpha}\delta\partial_x u - \delta^2(\underline{\gamma}^u)^2 u - 2\delta(\underline{\gamma}^u)^2 u \\ 296 & - 2i\varepsilon S_1(f)\underline{\alpha}\partial_x u - 2i\varepsilon S_1(f)\underline{\alpha}\delta\partial_x u - \varepsilon S_1(f)\delta^2(\underline{\gamma}^u)^2 u \\ 297 & - 2\varepsilon S_1(f)\delta(\underline{\gamma}^u)^2 u - \varepsilon S_1(f)(\underline{\gamma}^u)^2 u \\ 298 & - 2i\varepsilon^2 S_2(f)\underline{\alpha}\partial_x u - 2i\varepsilon^2 S_2(f)\underline{\alpha}\delta\partial_x u - \varepsilon^2 S_2(f)\delta^2(\underline{\gamma}^u)^2 u \\ 299 & - 2\varepsilon^2 S_2(f)\delta(\underline{\gamma}^u)^2 u - \varepsilon^2 S_2(f)(\underline{\gamma}^u)^2 u, \end{aligned}$$

301 and

$$302 \quad (5.8) \quad \tilde{J} = -\frac{1}{a}(\varepsilon f(x))T^u[u(x, a)],$$

303 and

$$304 \quad (5.9) \quad \tilde{H} = \varepsilon(\partial_x f)\partial_x u(x, 0) + \varepsilon\frac{f}{a}G(\varepsilon f)[U] - \varepsilon^2\frac{f(\partial_x f)}{a}\partial_x u(x, 0) - \varepsilon^2(\partial_x f)^2\partial_z u(x, 0).$$

305 It is not difficult to see that the forms for the  $A_j$ ,  $B_j$ , and  $S_j$  are

$$306 \quad A_0 = \begin{pmatrix} 1 & 0 \\ 0 & 1 \end{pmatrix},$$

$$307 \quad A_1(f) = \frac{1}{a} \begin{pmatrix} -2f & -(a-z)(\partial_x f) \\ -(a-z)(\partial_x f) & 0 \end{pmatrix},$$

$$308 \quad A_2(f) = \frac{1}{a^2} \begin{pmatrix} f^2 & (a-z)f(\partial_x f) \\ (a-z)f(\partial_x f) & (a-z)^2(\partial_x f)^2 \end{pmatrix},$$

309

310 and

$$311 \quad B_1(f) = \frac{1}{a} \begin{pmatrix} \partial_x f \\ 0 \end{pmatrix}, \quad B_2(f) = \frac{1}{a^2} \begin{pmatrix} -f(\partial_x f) \\ -(a-z)(\partial_x f)^2 \end{pmatrix},$$

312 and

$$313 \quad S_0 = 1, \quad S_1(f) = -\frac{2}{a}f, \quad S_2(f) = \frac{1}{a^2}f^2.$$

314 At this point we posit the expansions

$$315 \quad u(x, z; \varepsilon, \delta) = \sum_{n=0}^{\infty} \sum_{m=0}^{\infty} u_{n,m}(x, z) \varepsilon^n \delta^m, \quad G(\varepsilon, \delta) = \sum_{n=0}^{\infty} \sum_{m=0}^{\infty} G_{n,m} \varepsilon^n \delta^m,$$

316 and, upon insertion into (5.5) and (5.6), we find

$$317 \quad (5.10a) \quad \Delta u_{n,m} + 2i\alpha \partial_x u_{n,m} + (\underline{\gamma}^u)^2 u_{n,m} = \tilde{F}_{n,m}(x, z), \quad 0 < z < a,$$

$$318 \quad (5.10b) \quad u_{n,m}(x, 0) = \delta_{n,0} \delta_{m,0} U(x), \quad z = 0,$$

$$319 \quad (5.10c) \quad \partial_z u_{n,m}(x, a) - T^u[u_{n,m}(x, a)] = \tilde{J}_{n,m}(x), \quad z = a,$$

321 and

$$322 \quad (5.11) \quad G_{n,m}(f) = -\partial_z u_{n,m}(x, 0) + \tilde{H}_{n,m}(x).$$

323 The formulas for  $\tilde{F}_{n,m}$ ,  $\tilde{J}_{n,m}$  and  $\tilde{H}_{n,m}$  can be readily derived from (5.7), (5.8), and  
324 (5.9) above.

325 *Remark 5.1.* In a forthcoming publication we will use the recursions (5.10) and  
326 (5.11) to establish the *joint* analyticity of the DNO with respect to both interfacial  
327 and frequency deformations.

328 **5.1. Joint Expansion of Surface Data.** In order to specify forms for the  
329 surface data,  $\{\zeta_{n,m}, \psi_{n,m}\}$ , we require some results from [40]. First we recall the  
330 Taylor series expansion of the quantity  $\gamma_p^q$ , (2.3), with respect to  $\delta$  away from a  
331 Rayleigh singularity (Wood anomaly)  $\underline{\gamma}_p^q = 0$ .

332 **LEMMA 5.2.** [40] *The quantity  $\gamma_p^q$  has Taylor series expansion*

$$333 \quad \gamma_p^q(\delta) = \sum_{m=0}^{\infty} \gamma_{p,m}^q \delta^m,$$

334 where,

$$335 \quad \gamma_{p,0}^q = \pm \underline{\gamma}_p^q,$$

336 which we assume to be non-zero, giving rise to

$$337 \quad \gamma_{p,1}^q = \frac{2((k^q)^2 - \alpha \alpha_p)}{2\gamma_{p,0}^q}, \quad \gamma_{p,2}^q = \frac{(\underline{\gamma}^q)^2 - (\gamma_{p,1}^q)^2}{2\gamma_{p,0}^q},$$

$$338 \quad \gamma_{p,m}^q = \frac{-\sum_{r=1}^{m-1} \gamma_{p,m-r}^q \gamma_{p,r}^q}{2\gamma_{p,0}^q}, \quad m > 2.$$

339

340 *Remark 5.3.* As we noted in [40] we must be *away* from a Rayleigh singularity,  
 341  $\underline{\gamma}_p^q = 0$ , for *all*  $p$  in order for our expansion to be valid. See the final section of [40] for  
 342 a discussion of the behavior of the function  $\gamma_p^q(\delta)$  in the neighborhood of a Rayleigh  
 343 singularity.

344 Next we require the expansion of the composition of the exponential function  
 345 with the product of a function of  $\varepsilon$  and a function of  $\delta$  *jointly* in  $\varepsilon$  and  $\delta$ .

346 LEMMA 5.4. [40] Let  $\mathcal{E}(g, V) := \exp(g(x)V(\delta))$  for a function  $g(x)$  and an ana-  
 347 lytic function

$$348 \quad V = V(\delta) = \sum_{m=0}^{\infty} V_m \delta^m.$$

349 The composite function  $\mathcal{E}(g, V) = \mathcal{E}(\varepsilon f, V(\delta))$  is jointly analytic and has the Taylor  
 350 series expansion

$$351 \quad \mathcal{E}(\varepsilon, \delta) = \sum_{n=0}^{\infty} \sum_{m=0}^{\infty} \mathcal{E}_{n,m} \varepsilon^n \delta^m,$$

352 where

$$353 \quad \mathcal{E}_{n,m} = \begin{cases} 1, & n = m = 0, \\ 0, & n = 0, m > 0, \\ (V_0)^n \frac{f^n}{n!}, & n > 0, m = 0, \\ \frac{f}{n+1} \sum_{r=0}^m \mathcal{E}_{n,m-r} V_r, & n, m > 0. \end{cases}$$

354 *Remark 5.5.* We note that this latter Lemma can be effectively used to compute  
 355 the expansions of the functions

$$356 \quad e^{\pm i \gamma_p^q(\delta) \varepsilon f} = \mathcal{E}_p(\varepsilon f, \pm i \gamma_p^q(\delta)) = \mathcal{E}_p^{q,\pm}(\varepsilon, \delta) = \sum_{n=0}^{\infty} \sum_{m=0}^{\infty} \mathcal{E}_{p,n,m}^{q,\pm} \varepsilon^n \delta^m, \quad q \in \{u, w\},$$

357 which we presently require.

358 Using this Lemma we find Taylor expansions for the data generated by plane-wave  
 359 incidence (2.1e) and (2.1f). More specifically, for

$$360 \quad \zeta = \sum_{n=0}^{\infty} \sum_{m=0}^{\infty} \zeta_{n,m} \varepsilon^n \delta^m, \quad \psi = \sum_{n=0}^{\infty} \sum_{m=0}^{\infty} \psi_{n,m} \varepsilon^n \delta^m,$$

361 we have

$$362 \quad \zeta_{n,m} = -\mathcal{E}_{0,n,m}^{u,-},$$

$$363 \quad \psi_{n,m} = \sum_{r=0}^m (i \gamma_{p,m-r}^u) \mathcal{E}_{0,n,r}^{u,-} + (\partial_x f)(i \underline{\alpha}) \mathcal{E}_{0,n-1,m}^{u,-} + (\partial_x f)(i \underline{\alpha}) \mathcal{E}_{0,n-1,m-1}^{u,-}.$$

364

365 **6. Numerical Results.** We are now in a position to test a numerical implemen-  
 366 tation of our method and demonstrate its advantageous computational complexity.  
 367 Regarding the algorithm, our HOPS/AWE scheme is a High-Order Spectral method  
 368 [25, 6, 56] in the same spirit as our related Transformed Field Expansion (TFE) al-  
 369 gorithm [47], where nonlinearities are approximated with convolutions implemented

370 via the fast Fourier transform (FFT) algorithm. To test its validity we compare  
 371 simulations from our implementation of this HOPS/AWE method to exact solutions  
 372 constructed from the Method of Manufactured Solutions.

373 **6.1. Implementation.** As we mentioned above, our formulation of the scatter-  
 374 ing problem is

$$375 \quad \mathbf{A}(\varepsilon, \delta)\mathbf{V}(\varepsilon, \delta) = \mathbf{R}(\varepsilon, \delta),$$

376 c.f. (3.1), and our HOPS/AWE approach asks for the joint expansion of the  $\{\mathbf{A}, \mathbf{V}, \mathbf{R}\}$   
 377 in Taylor series, c.f. (4.1), where the  $\{\mathbf{V}_{n,m}\}$  satisfy equation (4.2). In our approxi-  
 378 mation we begin by truncating the Taylor series

$$379 \quad \{\mathbf{A}, \mathbf{V}, \mathbf{R}\}(\varepsilon, \delta) \approx \{\mathbf{A}^{N,M}, \mathbf{V}^{N,M}, \mathbf{R}^{N,M}\}(\varepsilon, \delta)$$

$$380 \quad (6.1) \quad := \sum_{n=0}^N \sum_{m=0}^M \{\mathbf{A}_{n,m}, \mathbf{V}_{n,m}, \mathbf{R}_{n,m}\} \varepsilon^n \delta^m,$$

$$381$$

382 and all that remains is to specify (i.) how the forms  $\mathbf{A}_{n,m}$  and  $\mathbf{R}_{n,m}$  in (4.3) are  
 383 simulated, and (ii.) how the operator  $\mathbf{A}_{0,0}$  is to be inverted.

384 For the latter we note that  $\mathbf{A}_{0,0}$  is diagonalized by the Fourier transform so that  
 385  $\mathbf{A}_{0,0}\mathbf{V}_{n,m} = \mathbf{Q}_{n,m}$  can be expressed as

$$386 \quad \sum_{p=-\infty}^{\infty} \widehat{\mathbf{A}}_{0,0}(p) \widehat{\mathbf{V}}_{n,m}(p) e^{i\bar{p}x} = \sum_{p=-\infty}^{\infty} \widehat{\mathbf{Q}}_{n,m}(p) e^{i\bar{p}x},$$

387 which implies

$$388 \quad \widehat{\mathbf{V}}_{n,m}(p) = \left[ \widehat{\mathbf{A}}_{0,0}(p) \right]^{-1} \widehat{\mathbf{Q}}_{n,m}(p).$$

389 It is not difficult to see [39] that

$$390 \quad \widehat{\mathbf{A}}_{0,0}(p) = \begin{pmatrix} 1 & -1 \\ (-i\gamma_p^u) & \tau^2(-i\gamma_p^w) \end{pmatrix},$$

391 c.f. (4.3), implying that

$$392 \quad \left[ \widehat{\mathbf{A}}_{0,0}(p) \right]^{-1} = \frac{1}{\Delta_p} \begin{pmatrix} \tau^2(-i\gamma_p^w) & 1 \\ (i\gamma_p^u) & 1 \end{pmatrix}, \quad \Delta_p := -(i\gamma_p^u + \tau^2(i\gamma_p^w)).$$

$$393$$

394 *Remark 6.1.* From these formulas it becomes obvious that the operator  $\mathbf{A}_{0,0}$  is  
 395 always invertible and our algorithm is well-defined. Recalling that we assume a  
 396 dielectric in the upper layer (so that the incident radiation propagates) we have that  
 397  $\gamma_p^u$  is either real and positive or purely imaginary (with positive imaginary part). If  
 398 a dielectric fills the lower layer then we have the same state of affairs for  $\gamma_p^w$  so that,  
 399 given that  $\tau^2$  will be positive and real,  $\Delta_p \neq 0$ . Alternatively, if a metal fills the lower  
 400 layer then  $\gamma_p^w$  will be complex with positive imaginary part. While it is less obvious,  
 401 this ensures that, once again,  $\Delta_p \neq 0$ .

402 Regarding the forms  $\mathbf{A}_{n,m}$  and  $\mathbf{R}_{n,m}$ , these boil down to the simulation of the  
 403 terms  $G_{n,m}$  and  $J_{n,m}$  in Taylor series approximations of the DNOs,  $G$  and  $J$ . There

404 is a large literature on the simulation of these operators in the case of a *boundary*  
 405 *perturbation* alone (see, e.g., [44]), however, a novelty of our current work is the  
 406 approximation of these DNOs *jointly* in interface and frequency deformation from the  
 407 recursions found in Section 5. As we presently describe, the method is very similar to  
 408 that presented in [44] save that additional elliptic solves are required.

409 **6.2. A Fourier/Chebyshev Collocation Discretization.** Focusing on the  
 410 upper layer DNO,  $G$ , we begin by approximating

$$411 \quad u(x, z; \varepsilon, \delta) \approx u^{N,M}(x, z; \varepsilon, \delta) := \sum_{n=0}^N \sum_{m=0}^M u_{n,m}(x, z) \varepsilon^n \delta^m.$$

412 Each of these  $u_{n,m}(x, z)$  are then simulated by a Fourier–Chebyshev approach which  
 413 posits the form

$$414 \quad u_{n,m}(x, z) \approx u_{n,m}^{N_x, N_z}(x, z) := \sum_{p=-N_x/2}^{N_x/2-1} \sum_{\ell=0}^{N_z} \hat{u}_{n,m,p,\ell} e^{i\tilde{p}x} T_\ell \left( \frac{2z-a}{a} \right),$$

415 where  $T_\ell$  is the  $\ell$ -th Chebyshev polynomial. The unknowns,  $\hat{u}_{n,m,p,\ell}$  are recovered  
 416 from (5.10) by the collocation approach [25, 14, 6, 56, 57]. With this we can simulate  
 417 the upper layer DNO from (5.11), giving

$$418 \quad G(x; \varepsilon, \delta) \approx G^{N,M}(x; \varepsilon, \delta) := \sum_{n=0}^N \sum_{m=0}^M G_{n,m}(x) \varepsilon^n \delta^m,$$

419 where

$$420 \quad (6.2) \quad G_{n,m}(x) \approx G_{n,m}^{N_x}(x) := \sum_{p=-N_x/2}^{N_x/2-1} \hat{G}_{n,m,p} e^{i\tilde{p}x},$$

421 and the  $\hat{G}_{n,m,p}$  are recovered from the  $\hat{u}_{n,m,p,\ell}$ .

422 **6.3. Padé Approximation.** We conclude our discussion of implementation  
 423 with consideration of how the Taylor series in  $(\varepsilon, \delta)$  are summed. For example, re-  
 424 garding the DNO,  $G$ , the approximation of  $\hat{G}_p(\varepsilon, \delta)$  by

$$425 \quad \hat{G}_p^{N,M}(\varepsilon, \delta) := \sum_{n=0}^N \sum_{m=0}^M \hat{G}_{n,m,p} \varepsilon^n \delta^m,$$

426 c.f. (6.2). The technique of Padé approximation [3] has been used with HOPS methods  
 427 to great advantage in the past [8, 45] and we advocate its use here. Classically, this  
 428 approach seeks to estimate the truncated Taylor series of a *single* variable

$$429 \quad Q^N(\rho) := \sum_{n=0}^N Q_n \rho^n \approx Q(\rho),$$

430 by the rational function

$$431 \quad [L/M](\rho) := \frac{a^L(\rho)}{b^M(\rho)} = \frac{\sum_{\ell=0}^L a_\ell \rho^\ell}{1 + \sum_{m=1}^M b_m \rho^m}, \quad L + M = N,$$

432 and

433 
$$[L/M](\rho) = Q^N(\rho) + \mathcal{O}(\rho^{L+M+1});$$

434 well-known formulas for the coefficients  $\{a_\ell, b_m\}$  can be found in [3]. Padé approx-  
 435 imation enjoys greatly enhanced convergence properties and we refer the interested  
 436 reader to § 2.2 of Baker & Graves–Morris [3] and the insightful calculations of § 8.3  
 437 of Bender & Orszag [4] for a thorough discussion of the capabilities and limitations  
 438 of Padé approximants.

439 In the current context of functions analytic with respect to *two* perturbation  
 440 variables we utilize the polar coordinates

441 
$$\varepsilon = \rho \cos(\theta), \quad \delta = \rho \sin(\theta),$$

442 and write the function

443 
$$\hat{G}_p(\varepsilon, \delta) = \sum_{n=0}^{\infty} \sum_{m=0}^{\infty} \hat{G}_{n,m,p} \varepsilon^n \delta^m$$
  
 444 
$$= \sum_{n=0}^{\infty} \sum_{m=0}^{\infty} \left( \hat{G}_{n,m,p} \cos^n(\theta) \sin^m(\theta) \right) \rho^{n+m}.$$
  
 445

446 Setting  $\ell = n + m$  and  $s = m$  we can write this as

447 
$$\hat{G}_p(\varepsilon, \delta) = \sum_{\ell=0}^{\infty} \left\{ \sum_{s=0}^{\ell} \hat{G}_{\ell-s,s,p} \cos^{\ell-s}(\theta) \sin^s(\theta) \right\} \rho^\ell =: \sum_{\ell=0}^{\infty} \tilde{G}_{\ell,p}(\theta) \rho^\ell.$$

448 We then chose particular values of  $\theta = \theta_j$  between 0 and  $2\pi$  and used classical Padé  
 449 approximation on the resulting  $\{\tilde{G}_{\ell,p}(\theta_j)\}$  as a function of  $\rho$  alone.

450 **6.4. The Domain of Analyticity.** In a forthcoming publication we will rig-  
 451 orously demonstrate the *joint* analyticity of the fields,  $\{u, w\}$ , DNOs,  $\{G, J\}$ , and  
 452 solutions,  $\{U, W\}$ , with respect to both boundary,  $\varepsilon$ , and frequency perturbations,  $\delta$ .  
 453 While this result requires that both  $\varepsilon$  and  $\delta$  be sufficiently small, we suspect that the  
 454 smallness requirement on  $\varepsilon$  can be removed, provided that it be real (see [45] for one  
 455 possible strategy). However, it is clear that no such extension exists for  $\delta$  as we have  
 456 already seen how the expansion for  $\gamma_p^q(\delta)$  fails at a Rayleigh Singularity,  $\underline{\gamma}_p^q = 0$ , c.f.  
 457 Lemma 5.2. Therefore the permissible values of  $\delta$  *must* be constrained by this.

458 To guide our computations we explore this restriction on  $\delta$  in more detail. For  
 459 instance, in the upper layer, Rayleigh singularities occur when  $\underline{\alpha}_p^2 = (\underline{k}^u)^2$  which  
 460 implies

461 (6.3) 
$$\underline{\omega} = \pm \frac{c_0}{n^u} \left\{ \underline{\alpha} + \frac{2\pi p}{d} \right\}, \quad \text{for any } p \in \mathbf{Z}.$$

462 In the interest of maximizing our choice of  $\delta$  we select a “mid–point” value of  $\underline{\omega}$  which  
 463 is as far away as possible from consecutive Rayleigh singularities

464 (6.4) 
$$\underline{\omega}_q := \frac{c_0}{n^u} \left\{ \underline{\alpha} + \frac{2\pi(q + 1/2)}{d} \right\}.$$

465 About this value the nearest singularities are

$$466 \quad \underline{\omega}_q^- := \frac{c_0}{n^u} \left\{ \underline{\alpha} + \frac{2\pi q}{d} \right\} = \underline{\omega}_q - \frac{\pi c_0}{n^u d},$$

$$467 \quad \underline{\omega}_q^+ := \frac{c_0}{n^u} \left\{ \underline{\alpha} + \frac{2\pi(q+1)}{d} \right\} = \underline{\omega}_q + \frac{\pi c_0}{n^u d},$$

468 so to maximize our range of  $\omega$  we choose, for some filling fraction  $0 < \sigma < 1$ ,

$$470 \quad \underline{\omega}_q - \sigma \left( \frac{\pi c_0}{n^u d} \right) < \omega < \underline{\omega}_q + \sigma \left( \frac{\pi c_0}{n^u d} \right).$$

471 To express this in terms of  $\delta$  we recall that  $\omega = (1 + \delta)\underline{\omega}_q$  which gives

$$472 \quad -\sigma \left( \frac{\pi c_0}{\underline{\omega}_q n^u d} \right) < \delta < \sigma \left( \frac{\pi c_0}{\underline{\omega}_q n^u d} \right).$$

473 Simplifying gives

$$474 \quad (6.5) \quad -\left( \frac{\sigma}{(\underline{\alpha}d/\pi) + 2q + 1} \right) < \delta < \left( \frac{\sigma}{(\underline{\alpha}d/\pi) + 2q + 1} \right).$$

475 **6.5. Validation by the Method of Manufactured Solutions.** To validate  
476 our scheme we utilized the Method of Manufactured Solutions [13, 53, 54]. To sum-  
477 marize, consider the general system of partial differential equations subject to generic  
478 boundary conditions

$$479 \quad \mathcal{P}v = 0, \quad \text{in } \Omega,$$

$$480 \quad \mathcal{B}v = 0, \quad \text{at } \partial\Omega.$$

482 It is typically easy to implement a numerical algorithm to solve the nonhomogeneous  
483 version of this set of equations

$$484 \quad \mathcal{P}v = \mathcal{F}, \quad \text{in } \Omega,$$

$$485 \quad \mathcal{B}v = \mathcal{J}, \quad \text{at } \partial\Omega.$$

487 To test an implementation we began with the “manufactured solution,”  $\tilde{v}$ , and set

$$488 \quad \mathcal{F}_v := \mathcal{P}\tilde{v}, \quad \mathcal{J}_v := \mathcal{J}\tilde{v}.$$

489 Thus, given the pair  $\{\mathcal{F}_v, \mathcal{J}_v\}$  we had an *exact* solution of the nonhomogeneous prob-  
490 lem, namely  $\tilde{v}$ . While this does not prove an implementation to be correct, if the  
491 function  $\tilde{v}$  is chosen to imitate the behavior of anticipated solutions (e.g., satisfying  
492 the boundary conditions exactly) then this gives us confidence in our algorithm.

493 We considered the periodic, outgoing solutions of the Helmholtz equation (2.6a)

$$494 \quad u_r(x, z) := A_r e^{i\tilde{r}x + i\gamma_r^u z}, \quad r \in \mathbf{Z}, \quad A_r \in \mathbf{C},$$

495 and their counterparts for (2.6b)

$$496 \quad w_r(x, z) := B_r e^{i\tilde{r}x - i\gamma_r^w z}, \quad r \in \mathbf{Z}, \quad B_r \in \mathbf{C}.$$

497 We selected the simple sinusoidal profile

$$498 \quad (6.6) \quad g(x) = \varepsilon f(x) = \varepsilon \left( \frac{\cos(4x)}{4} \right),$$

499 and defined the Dirichlet and Neumann traces

$$500 \quad (6.7a) \quad U_r(x) := u_r(x, g(x)), \quad \tilde{U}_r(x) := -\partial_N u_r(x, g(x)),$$

$$501 \quad (6.7b) \quad W_r(x) := w_r(x, g(x)), \quad \tilde{W}_r(x) := \partial_N w_r(x, g(x)).$$

503 From these we defined the two-layer data to be provided to our algorithm

$$504 \quad (6.7c) \quad \zeta_r := U_r - W_r, \quad \psi_r := -\tilde{U}_r - \tau^2 \tilde{W}_r.$$

505 We chose the following physical parameters

$$506 \quad (6.8) \quad d = 2\pi, \quad \alpha = 0, \quad \epsilon^u = 1, \quad \epsilon^w = 1.1, \quad r = 4, \quad A_r = 5, \quad B_r = 3,$$

507 in TM polarization, and the numerical parameters

$$508 \quad (6.9) \quad N_x = 32, \quad N_z = 32, \quad a = 1, \quad b = -1.$$

509 With a rescaling of the frequency (e.g., via a change of the time variable,  $t' = t/c_0$ )  
510 we arrange for  $c_0 = 1$  and considered the base frequency

$$511 \quad \underline{\omega}_1 = 3/2,$$

512 and filling fraction  $\sigma = 0.99$ .

513 To illuminate the behavior of our scheme we studied four choices of the numerical  
514 parameter

$$515 \quad N = M = 4, 8, 12, 16,$$

516 and the physical quantities

$$517 \quad \varepsilon = 10^{-2}, 10^{-4}, 10^{-6}, 10^{-8},$$

518 in (6.6). For this we supplied the “exact” input data,  $\{\zeta_r, \psi_r\}$ , from (6.7) to our  
519 HOPS/AWE algorithm to simulate solutions of the two-layer problem giving  $\{U_r^{\text{approx}}, W_r^{\text{approx}}\}$ .  
520 We compared this with the “exact” solutions  $\{U_r^{\text{exact}}, W_r^{\text{exact}}\}$  and computed the rel-  
521 ative error

$$522 \quad \text{Error}_{\text{rel}} := \frac{|U_r^{\text{exact}} - U_r^{\text{approx}}|_{\infty}}{|U_r^{\text{exact}}|_{\infty}}.$$

523 We point out that measuring the defect in the upper-layer Dirichlet data was arbitrary  
524 and we noticed similar behavior for the lower-layer analogue.

525 We report our results of these simulations in Figures 2 and 3. More specifically,  
526 Figure 2 displays both the rapid and stable decay of the relative error for fixed  $N$  and  
527  $M$ , and how this rate of decay improves as  $(\varepsilon, \delta)$  decrease. Figure 3 shows both how  
528 the error shrinks as  $(\varepsilon, \delta)$  become smaller, and that this rate is enhanced as both  $N$   
529 and  $M$  are increased.

530 **6.6. Simulations of the Reflectivity Maps.** In Section 2.2 we defined the  
531 Reflectivity Map  $R = R(\varepsilon, \delta)$ , c.f. (2.7). Using our novel HOPS/AWE approach we  
532 computed

$$533 \quad R_{\text{HOPS/AWE}}^{N, M, N_x, N_z} \approx R,$$



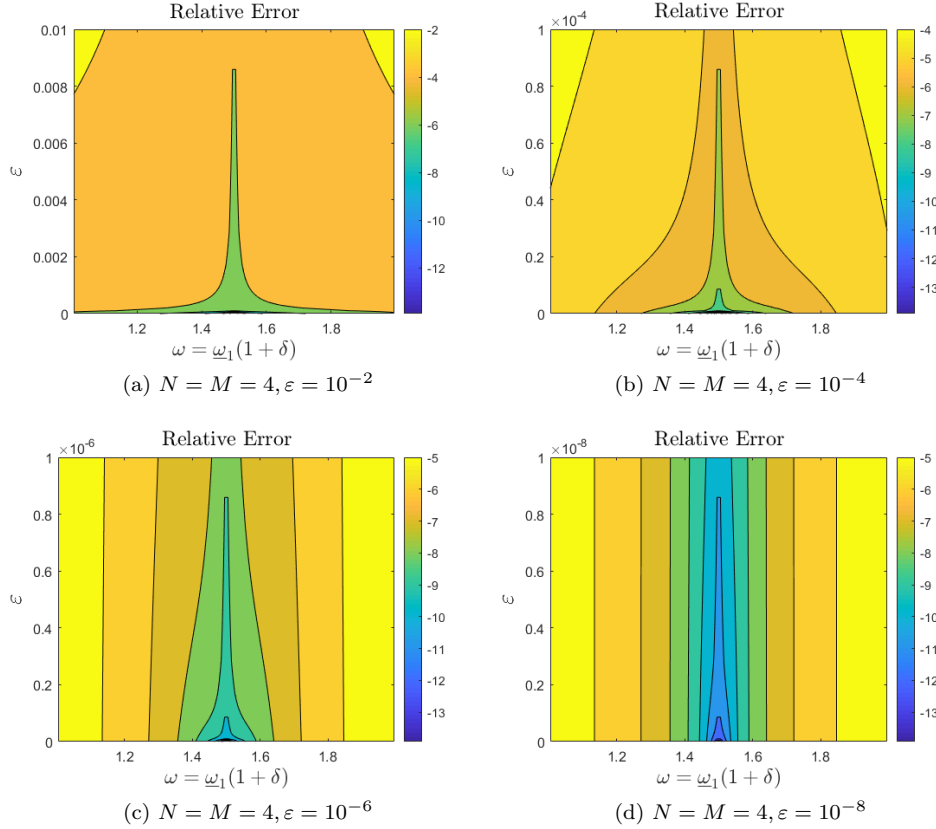


Fig. 2: Plot of relative error with fixed  $N = M = 4$  and four choices of  $\varepsilon = 10^{-2}, 10^{-4}, 10^{-6}, 10^{-8}$  with Taylor summation. Physical parameters were (6.8) and numerical discretization was (6.9).

534 for a range of  $\varepsilon$  and  $\delta$ . As in our previous work [40], we show the kind of simula-  
 535 tions this HOPS/AWE method can produce with modest computational effort. For  
 536 this we selected  $\omega_q$ , c.f. (6.4), for  $1 \leq q \leq 6$  and simulated  $R$  in the following fre-  
 537 quency/wavelength ranges

538	$q = 1 : \omega \in [1.005, 1.995]$	$\implies$	$\lambda \in [3.14947, 6.25193]$ ,
539	$q = 2 : \omega \in [2.005, 2.995]$	$\implies$	$\lambda \in [2.09789, 3.13376]$ ,
540	$q = 3 : \omega \in [3.005, 3.995]$	$\implies$	$\lambda \in [1.57276, 2.09091]$ ,
541	$q = 4 : \omega \in [4.005, 4.995]$	$\implies$	$\lambda \in [1.25789, 1.56884]$ ,
542	$q = 5 : \omega \in [5.005, 5.995]$	$\implies$	$\lambda \in [1.04807, 1.25538]$ ,
543	$q = 6 : \omega \in [6.005, 6.995]$	$\implies$	$\lambda \in [0.89824, 1.04633]$ ,
544			

545 c.f. (6.5). In addition, we selected

546 
$$g(x) = \varepsilon f(x), \quad f(x) = \cos(x), \quad \varepsilon_{\max} = 0.2,$$

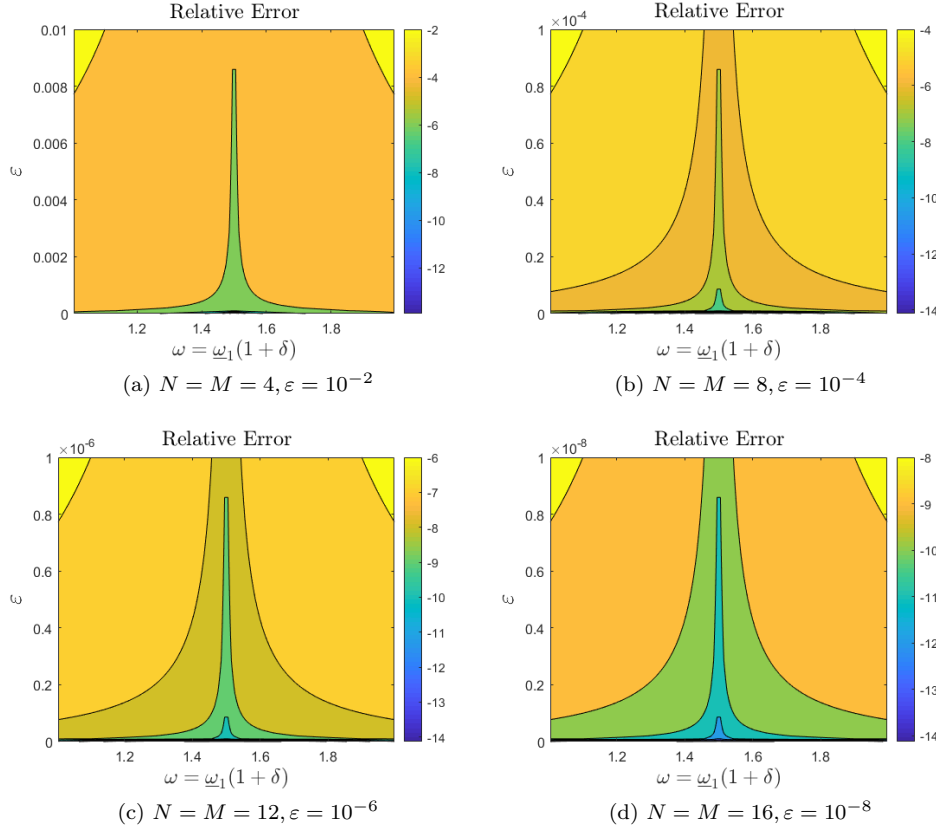


Fig. 3: Plot of relative error with four choices of  $N = M = 4, 8, 12, 16$  and four choices of  $\varepsilon = 10^{-2}, 10^{-4}, 10^{-6}, 10^{-8}$  with Taylor summation. Physical parameters were (6.8) and numerical discretization was (6.9).

547 with the parameters

548 
$$\alpha = 0, \quad \sigma = 0.99, \quad n^u = 1, \quad n^w = 1.1, \quad N_x = 32, \quad N = M = 16.$$

549 In Figure 4(a) we plot all six of these subsets of the Reflectivity Map on one set of  
 550 coordinate axes, and in Figure 4(b) we plot the energy defect,  $D$ , (2.8), to verify the  
 551 accuracy of our expansions.

552 We then changed the lower index of refraction  $n^w$  to match representative values  
 553 of silver and gold as reported by Johnson & Christy [30], in particular

554 
$$n_{\text{Ag}} = 0.05 + 2.275i, \quad n_{\text{Au}} = 1.48 + 1.883i.$$

555 Using the same frequency and wavelength ranges, we studied

556 
$$f(x) = \cos(4x), \quad \varepsilon_{\text{max}} = 0.2,$$

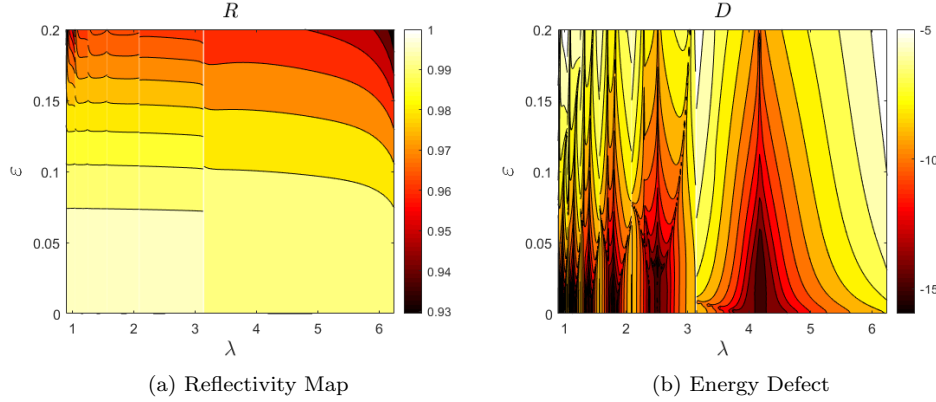


Fig. 4: The Reflectivity Map,  $R(\varepsilon, \delta)$ , and energy defect  $D$  computed with our HOPS/AWE algorithm with Taylor summation. We set  $N = M = 16$  with a granularity of  $N_\varepsilon = N_\delta = 100$  per invocation. Parameter choices were  $\alpha = 0$ ,  $\sigma = 0.99$ ,  $n^u = 1$ ,  $n^w = 1.1$ , and  $N_x = 32$ .

557 with the parameters

558  $\alpha = 0, \quad \sigma = 0.99, \quad n^u = 1, \quad N_x = 32, \quad N = M = 15.$

In Figure 5(a) we plot six different subsets of the reflectivity map where the lower

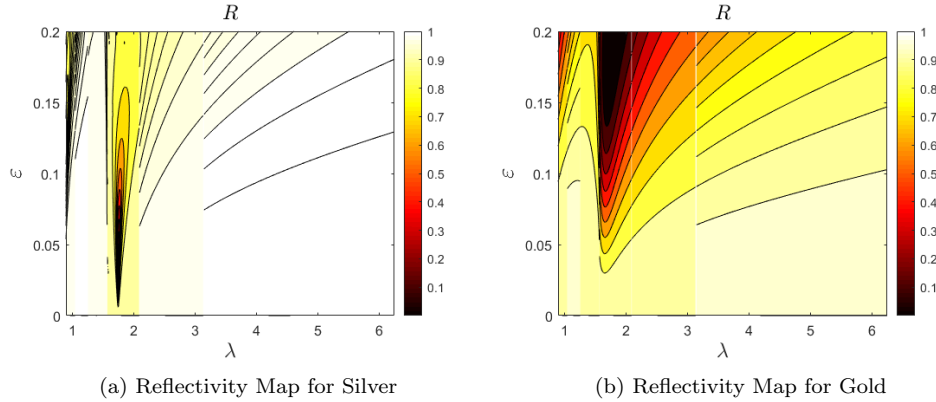


Fig. 5: The Reflectivity Map,  $R(\varepsilon, \delta)$ , for silver (left) and gold (right) with Padé summation. We set  $N = M = 15$  with a granularity of  $N_\varepsilon = N_\delta = 100$  per invocation. Parameter choices were  $\alpha = 0$ ,  $\sigma = 0.99$ ,  $n^u = 1$ ,  $n^w = n_{Ag}$  (left) and  $n^w = n_{Au}$  (right),  $N_x = 32$ , and the periodicity of the grating was selected as  $d = 2\pi$ .

559  
 560 index of refraction is selected to model the optical constant of silver. In Figure 5(b) we  
 561 plot six different subsets of the Reflectivity Map where the lower index of refraction  
 562 is changed to the optical constant for gold.

563 In the next set of simulations we dropped the assumptions that  $d = 2\pi$  and  $c_0$  is  
 564 unity. We calculated the Reflectivity Map for a silver grating with a sinusoidal profile

$$565 \quad g(x) = \varepsilon f(x), \quad f(x) = \frac{1}{4} \sin\left(\frac{4\pi x}{d}\right), \quad d = 0.28\mu\text{m}, \quad \varepsilon_{\max} = 0.2,$$

566 with the parameters

$$567 \quad \alpha = 0, \quad \sigma = 0.99, \quad n^u = 1, \quad n^w = n_{\text{Ag}}, \quad N_x = 32,$$

568 and  $N = M = 4, 8, 12, 16$ . In Figure 6 we plot a single subset of the Reflectivity Map  
 569 corresponding to our parameter choices for silver. The combined plots show that as  
 both  $N$  and  $M$  become larger, our HOPS/AWE algorithm converges.

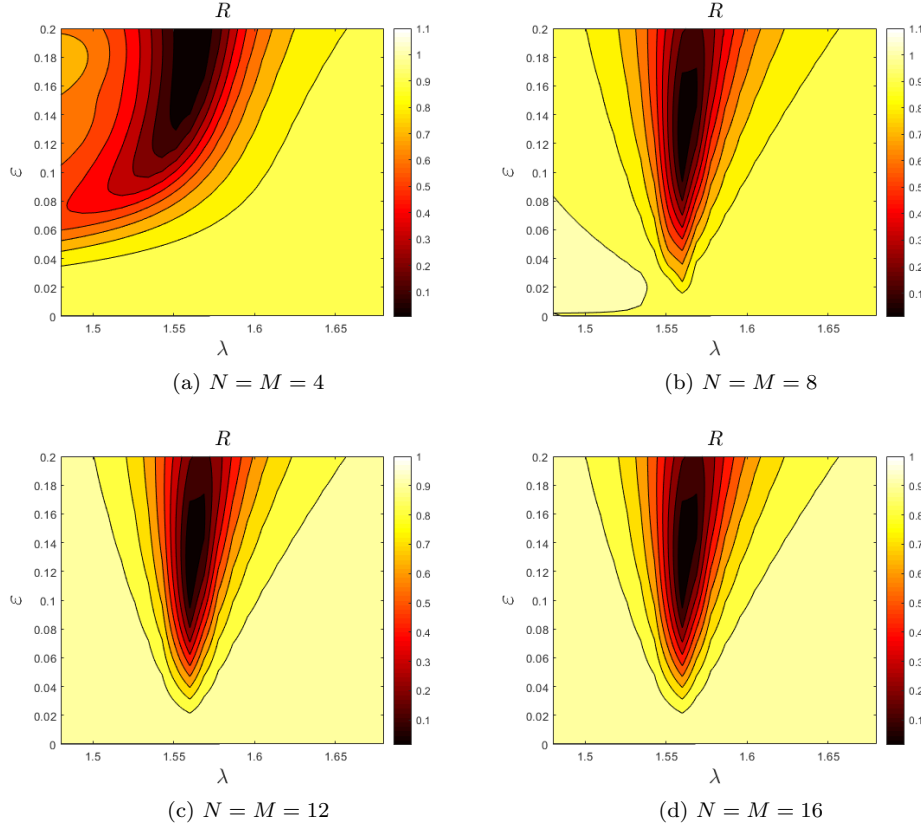


Fig. 6: The Reflectivity Map,  $R(\varepsilon, \delta)$ , for silver with Padé summation. We set  $N = M = 4, 8, 12, 16$  with a granularity of  $N_\varepsilon = N_\delta = 100$  per invocation. Parameter choices were  $\alpha = 0, \sigma = 0.99, n^u = 1, n^w = n_{\text{Ag}}, N_x = 32$ , and the periodicity of the grating was selected as  $d = 0.28\mu\text{m}$ .

570

571 We conclude with simulations of non-normal incidence ( $\alpha \neq 0$ ) and we return to  
 572 the case  $d = 2\pi$  and unit  $c_0$ . Recalling the Rayleigh singularity condition, (6.4), we  
 573 note the dependence on not only  $n^u$  but also  $\alpha$ . With this in mind we revisited the

574 Reflectivity Map simulations from the beginning of the section in neighborhoods of  
 575  $\omega_q$ ,  $1 \leq q \leq 3$ , giving rise to frequency/wavelength ranges

$$\begin{aligned}
 576 \quad & q = 1 : \quad \omega \in [1.005, 1.995] \quad \implies \quad \lambda \in [3.14947, 6.25193], \\
 577 \quad & q = 2 : \quad \omega \in [2.005, 2.995] \quad \implies \quad \lambda \in [2.09789, 3.13376], \\
 578 \quad & q = 3 : \quad \omega \in [3.005, 3.995] \quad \implies \quad \lambda \in [1.57276, 2.09091].
 \end{aligned}$$

580 We selected

$$581 \quad f(x) = \sin(3x), \quad \varepsilon_{\max} = 0.1,$$

582 with the parameters

$$583 \quad \alpha = 0.1, \quad \sigma = 0.99, \quad n^u = 1, \quad n^w = 2.3782, \quad N_x = 64, \quad N = M = 13,$$

584 and the value of  $n^w$  is meant to model carbon [50]. In Figure 7(a) we plot three  
 585 different subsets of the reflectivity map on one set of coordinate axes. In Figure 7(b)  
 586 we plot the energy defect, (2.8), to show the accuracy of our scheme in the case  $\alpha \neq 0$ .

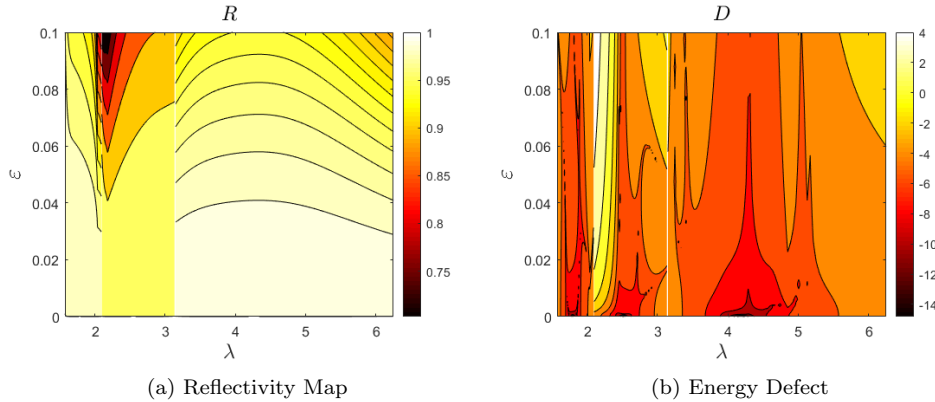


Fig. 7: The Reflectivity Map,  $R(\varepsilon, \delta)$ , and energy defect  $D$  computed with our HOPS/AWE algorithm with Taylor summation. We set  $N = M = 13$  with a granularity of  $N_\varepsilon = N_\delta = 100$  per invocation. Parameter choices were  $\alpha = 0.1$ ,  $\sigma = 0.99$ ,  $n^u = 1$ ,  $n^w = 2.3782$  (carbon), and  $N_x = 64$ .

587

588 We conclude with computations of the same configuration but with increased  
 589 granularity,  $N_\varepsilon = N_\delta = 1000$  per invocation. In the next section we discuss the  
 590 advantageous computational complexity our HOPS/AWE algorithm enjoys in this  
 591 situation of large  $N_\varepsilon$  and  $N_\delta$ . We selected

$$592 \quad f(x) = \cos(x), \quad \varepsilon_{\max} = 0.2,$$

593 with the parameters

$$594 \quad \alpha = 0.01, \quad \sigma = 0.99, \quad n^u = 1, \quad n^w = 1.1, \quad N_x = 32, \quad N = M = 16.$$

595 In Figure 8(a) we plot six different subsets of the Reflectivity Map on a single coordi-  
 596 nate axis, and in Figure 8(b) we plot the energy defect, (2.8), to demonstrate the  
 accuracy of our scheme with a nonzero value of  $\underline{\alpha}$ .

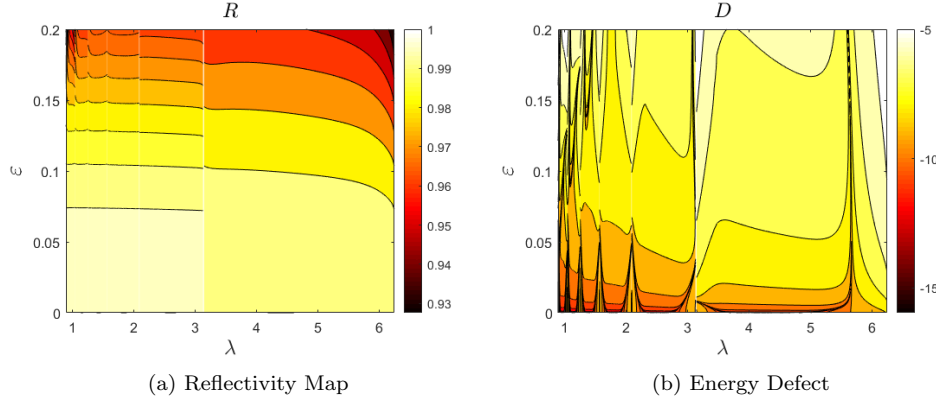


Fig. 8: The Reflectivity Map,  $R(\varepsilon, \delta)$ , and energy defect  $D$  computed with our HOPS/AWE algorithm with Taylor summation. We set  $N = M = 16$  with a granularity of  $N_\varepsilon = N_\delta = 1000$  per invocation. Parameter choices were  $\alpha = 0.01$ ,  $\sigma = 0.99$ ,  $n^u = 1$ ,  $n^w = 1.1$ , and  $N_x = 32$ .

597

598 **6.7. Computational Complexity.** One of the primary motivations for our  
 599 HOPS/AWE algorithm is its superior computational complexity for problems within  
 600 its domain of applicability. In comparison with classical BIE methods, for instance,  
 601 the HOPS/AWE approach has several advantages for computing QoIs like the Re-  
 602 flectivity Map,  $R = R(\varepsilon, \delta)$ . To demonstrate this we begin by fixing the problem of  
 603 computing  $R$  for  $N_\varepsilon$  many values of  $\varepsilon$  and  $N_\delta$  many values of  $\delta$ .

604 We recall from Section 6.2 that our HOPS/AWE algorithm requires  $N_x \times N_z$  un-  
 605 knowns at every perturbation order,  $(n, m)$ , corresponding to the  $N_x$  equally-spaced  
 606 gridpoints in the lateral direction and the  $N_z$  collocation points in the vertical dimen-  
 607 sion. A careful study of the HOPS/AWE recursions (4.2) reveals that the compu-  
 608 tational complexity of *forming* the right-hand side at order  $(n, m)$  (the most costly  
 609 step) is

$$610 \quad \mathcal{O}(nmN_x \log(N_x)N_z \log(N_z)).$$

611 Inverting the operator  $A_{0,0}$  has complexity  $\mathcal{O}(N_x \log(N_x)N_z \log(N_z))$  so the full cost  
 612 of computing the  $\{U_{n,m}, W_{n,m}\}$ ,  $\{0 \leq n \leq N, 0 \leq m \leq M\}$ , is

$$613 \quad \mathcal{O}(N^2M^2N_x \log(N_x)N_z \log(N_z)).$$

614 Once these coefficients are recovered, the cost of summing the series in  $(\varepsilon, \delta)$  is min-  
 615 imal, provided it is done in an efficient manner (e.g., by Horner's rule [12, 2]). Our  
 616 algorithm then requires an additional  $\mathcal{O}(N_\varepsilon N_\delta)$  steps to sum over every value of  $(\varepsilon, \delta)$ ,  
 617 therefore the *full* cost of computing the Reflectivity Map by our HOPS/AWE method  
 618 is

$$619 \quad \mathcal{O}(N^2M^2N_x \log(N_x)N_z \log(N_z) + N_\varepsilon N_\delta).$$

620 In contrast, for a single  $(\varepsilon, \delta)$  pair, a BIM solver with  $N_x$  lateral gridpoints requires  
 621 time proportional to  $\mathcal{O}(N_x^3)$  for Gaussian elimination to solve the resulting *dense*  
 622 system of  $N_x$  equations in  $N_x$  unknowns [12, 2, 17]. Applying this  $N_\varepsilon \times N_\delta$  times  
 623 results in a total computational complexity of

$$624 \quad \mathcal{O}(N_x^3 N_\varepsilon N_\delta).$$

625 Thus, once  $N_\varepsilon$  and  $N_\delta$  become large, e.g.,

$$626 \quad N_\varepsilon N_\delta > \frac{N^2 M^2 N_x \log(N_x) N_z \log(N_z)}{N_x^3},$$

627 our new algorithm becomes far more efficient.

628 **7. Conclusions.** In this paper we have described a novel, High-Order Spectral  
 629 [25, 14] High-Order Perturbation of Surfaces (HOPS)/Asymptotic Waveform Eval-  
 630 uation (AWE) method [40] which employs a perturbation approach to address the  
 631 geometric and frequency deviations from a base configuration. For quantities which  
 632 depend upon both of these variables, such as the Reflectivity Map, this method enjoys  
 633 extremely favorable computational complexity as compared with standard numerical  
 634 methods such as Finite Differences, Finite Elements, and even Integral Equations.  
 635 Our HOPS/AWE algorithm has been shown to be rapid, robust, and highly accurate.

636 **Acknowledgments.** D.P.N. gratefully acknowledges support from the National  
 637 Science Foundation through grants No. DMS-1813033 and No. DMS-2111283.

638

## REFERENCES

- 639 [1] T. ARENS, *Scattering by Biperiodic Layered Media: The Integral Equation Approach*, habilita-  
 640 tionsschrift, Karlsruhe Institute of Technology, 2009.
- 641 [2] K. ATKINSON AND W. HAN, *Theoretical numerical analysis*, vol. 39 of Texts in Applied Math-  
 642 ematics, Springer-Verlag, New York, 2001. A functional analysis framework.
- 643 [3] G. A. BAKER, JR. AND P. GRAVES-MORRIS, *Padé approximants*, Cambridge University Press,  
 644 Cambridge, second ed., 1996.
- 645 [4] C. M. BENDER AND S. A. ORSZAG, *Advanced mathematical methods for scientists and engi-  
 646 neers*, McGraw-Hill Book Co., New York, 1978. International Series in Pure and Applied  
 647 Mathematics.
- 648 [5] F. BLEIBINHAUS AND S. RONDENAY, *Effects of surface scattering in full-waveform inversion*,  
 649 *Geophysics*, 74 (2009), pp. WCC69–WCC77.
- 650 [6] J. P. BOYD, *Chebyshev and Fourier spectral methods*, Dover Publications Inc., Mineola, NY,  
 651 second ed., 2001.
- 652 [7] L. M. BREKHOVSKIKH AND Y. P. LYSANOV, *Fundamentals of Ocean Acoustics*, Springer-Verlag,  
 653 Berlin, 1982.
- 654 [8] O. BRUNO AND F. REITICH, *Numerical solution of diffraction problems: A method of variation  
 655 of boundaries. II. Finitely conducting gratings, Padé approximants, and singularities*, *J.  
 656 Opt. Soc. Am. A*, 10 (1993), pp. 2307–2316.
- 657 [9] O. P. BRUNO, M. LYON, C. PÉREZ-ARANCIBIA, AND C. TURC, *Windowed Green function method  
 658 for layered-media scattering*, *SIAM J. Appl. Math.*, 76 (2016), pp. 1871–1898.
- 659 [10] O. P. BRUNO, S. P. SHIPMAN, C. TURC, AND S. VENAKIDES, *Superalgebraically convergent  
 660 smoothly windowed lattice sums for doubly periodic Green functions in three-dimensional  
 661 space*, *Proc. A.*, 472 (2016), pp. 20160255, 19.
- 662 [11] O. P. BRUNO, S. P. SHIPMAN, C. TURC, AND S. VENAKIDES, *Three-dimensional quasi-periodic  
 663 shifted Green function throughout the spectrum, including Wood anomalies*, *Proc. A.*, 473  
 664 (2017), pp. 20170242, 18.
- 665 [12] R. BURDEN AND J. D. FAIRES, *Numerical analysis*, Brooks/Cole Publishing Co., Pacific Grove,  
 666 CA, sixth ed., 1997.
- 667 [13] O. R. BURGGRAF, *Analytical and numerical studies of the structure of steady separated flows*,  
 668 *J. Fluid Mech.*, 24 (1966), pp. 113–151.

- 669 [14] C. CANUTO, M. Y. HUSSAINI, A. QUARTERONI, AND T. A. ZANG, *Spectral methods in fluid*  
670 *dynamics*, Springer-Verlag, New York, 1988.
- 671 [15] J. CHANDEZON, M. DUPUIS, G. CORNET, AND D. MAYSTRE, *Multicoated gratings: a differential*  
672 *formalism applicable in the entire optical region*, J. Opt. Soc. Amer., 72 (1982), p. 839.
- 673 [16] J. CHANDEZON, D. MAYSTRE, AND G. RAOULT, *A new theoretical method for diffraction gratings*  
674 *and its numerical application*, J. Opt., 11 (1980), pp. 235–241.
- 675 [17] D. COLTON AND R. KRESS, *Inverse acoustic and electromagnetic scattering theory*, vol. 93 of  
676 Applied Mathematical Sciences, Springer, New York, third ed., 2013.
- 677 [18] COMSOL, *COMSOL Multiphysics Reference Manual*, COMSOL, Inc., Stockholm, Sweden,  
678 2019.
- 679 [19] B. DESPRÉS, *Domain decomposition method and the Helmholtz problem*, in Mathematical and  
680 numerical aspects of wave propagation phenomena (Strasbourg, 1991), SIAM, Philadelphia,  
681 PA, 1991, pp. 44–52.
- 682 [20] B. DESPRÉS, *Méthodes de décomposition de domaine pour les problèmes de propagation d’ondes*  
683 *en régime harmonique. Le théorème de Borg pour l’équation de Hill vectorielle*, Institut  
684 National de Recherche en Informatique et en Automatique (INRIA), Rocquencourt, 1991.  
685 Thèse, Université de Paris IX (Dauphine), Paris, 1991.
- 686 [21] M. O. DEVILLE, P. F. FISCHER, AND E. H. MUND, *High-order methods for incompressible*  
687 *fluid flow*, vol. 9 of Cambridge Monographs on Applied and Computational Mathematics,  
688 Cambridge University Press, Cambridge, 2002.
- 689 [22] T. W. EBBESEN, H. J. LEZEC, H. F. GHAEMI, T. THIO, AND P. A. WOLFF, *Extraordinary*  
690 *optical transmission through sub-wavelength hole arrays*, Nature, 391 (1998), pp. 667–669.
- 691 [23] S. ENOCH AND N. BONOD, *Plasmonics: From Basics to Advanced Topics*, Springer Series in  
692 Optical Sciences, Springer, New York, 2012.
- 693 [24] *Solids far from equilibrium*, Cambridge University Press, Cambridge, 1992.
- 694 [25] D. GOTTLIEB AND S. A. ORSZAG, *Numerical analysis of spectral methods: theory and applica-*  
695 *tions*, Society for Industrial and Applied Mathematics, Philadelphia, Pa., 1977. CBMS-NSF  
696 Regional Conference Series in Applied Mathematics, No. 26.
- 697 [26] J. S. HESTHAVEN AND T. WARBURTON, *Nodal discontinuous Galerkin methods*, vol. 54 of Texts  
698 in Applied Mathematics, Springer, New York, 2008. Algorithms, analysis, and applications.
- 699 [27] J. HOMOLA, *Surface plasmon resonance sensors for detection of chemical and biological species*,  
700 Chemical Reviews, 108 (2008), pp. 462–493.
- 701 [28] H. IM, S. H. LEE, N. J. WITTENBERG, T. W. JOHNSON, N. C. LINDQUIST, P. NAGPAL, D. J.  
702 NORRIS, AND S.-H. OH, *Template-stripped smooth Ag nanohole arrays with silica shells for*  
703 *surface plasmon resonance biosensing*, ACS Nano, 5 (2011), pp. 6244–6253.
- 704 [29] C. JOHNSON, *Numerical solution of partial differential equations by the finite element method*,  
705 Cambridge University Press, Cambridge, 1987.
- 706 [30] P. JOHNSON AND R. CHRISTY, *Optical constants of the noble metals*, Physical Review B, 6  
707 (1972), p. 4370.
- 708 [31] J. JOSE, L. R. JORDAN, T. W. JOHNSON, S. H. LEE, N. J. WITTENBERG, AND S.-H. OH,  
709 *Topographically flat substrates with embedded nanoplasmonic devices for biosensing*, Adv  
710 Funct Mater, 23 (2013), pp. 2812–2820.
- 711 [32] R. KRESS, *Linear integral equations*, Springer-Verlag, New York, third ed., 2014.
- 712 [33] R. J. LEVEQUE, *Finite difference methods for ordinary and partial differential equations*, Soci-  
713 *ety for Industrial and Applied Mathematics (SIAM), Philadelphia, PA, 2007. Steady-state*  
714 *and time-dependent problems.*
- 715 [34] P.-L. LIONS, *On the Schwarz alternating method. III. A variant for nonoverlapping subdo-*  
716 *main*, in Third International Symposium on Domain Decomposition Methods for Partial  
717 Differential Equations (Houston, TX, 1989), SIAM, Philadelphia, PA, 1990, pp. 202–223.
- 718 [35] S. A. MAIER, *Plasmonics: Fundamentals and Applications*, Springer, New York, 2007.
- 719 [36] M. MOSKOVITS, *Surface-enhanced spectroscopy*, Reviews of Modern Physics, 57 (1985), pp. 783–  
720 826.
- 721 [37] P. NAGPAL, N. C. LINDQUIST, S.-H. OH, AND D. J. NORRIS, *Ultrasmooth patterned metals for*  
722 *plasmonics and metamaterials*, Science, 325 (2009), pp. 594–597.
- 723 [38] F. NATTERER AND F. WÜBBELING, *Mathematical methods in image reconstruction*, SIAM  
724 Monographs on Mathematical Modeling and Computation, Society for Industrial and Ap-  
725 plied Mathematics (SIAM), Philadelphia, PA, 2001.
- 726 [39] D. P. NICHOLLS, *Three-dimensional acoustic scattering by layered media: A novel surface*  
727 *formulation with operator expansions implementation*, Proceedings of the Royal Society of  
728 London, A, 468 (2012), pp. 731–758.
- 729 [40] D. P. NICHOLLS, *Numerical solution of diffraction problems: A high-order perturbation of*  
730 *surfaces/asymptotic waveform evaluation method*, SIAM Journal on Numerical Analysis,



- 731 55 (2017), pp. 144–167.
- 732 [41] D. P. NICHOLLS, *On analyticity of linear waves scattered by a layered medium*, Journal of  
733 Differential Equations, 263 (2017), pp. 5042–5089.
- 734 [42] D. P. NICHOLLS, *Numerical simulation of grating structures incorporating two-dimensional*  
735 *materials: A high-order perturbation of surfaces framework*, SIAM Journal on Applied  
736 Mathematics, 78 (2018), pp. 19–44.
- 737 [43] D. P. NICHOLLS AND F. REITICH, *A new approach to analyticity of Dirichlet-Neumann opera-*  
738 *tors*, Proc. Roy. Soc. Edinburgh Sect. A, 131 (2001), pp. 1411–1433.
- 739 [44] D. P. NICHOLLS AND F. REITICH, *Stability of high-order perturbative methods for the compu-*  
740 *tation of Dirichlet-Neumann operators*, J. Comput. Phys., 170 (2001), pp. 276–298.
- 741 [45] D. P. NICHOLLS AND F. REITICH, *Analytic continuation of Dirichlet-Neumann operators*, Nu-  
742 mer. Math., 94 (2003), pp. 107–146.
- 743 [46] D. P. NICHOLLS AND F. REITICH, *Shape deformations in rough surface scattering: Cancellations,*  
744 *conditioning, and convergence*, J. Opt. Soc. Am. A, 21 (2004), pp. 590–605.
- 745 [47] D. P. NICHOLLS AND F. REITICH, *Shape deformations in rough surface scattering: Improved*  
746 *algorithms*, J. Opt. Soc. Am. A, 21 (2004), pp. 606–621.
- 747 [48] D. P. NICHOLLS AND M. TABER, *Joint analyticity and analytic continuation for Dirichlet-*  
748 *Neumann operators on doubly perturbed domains*, J. Math. Fluid Mech., 10 (2008),  
749 pp. 238–271.
- 750 [49] R. PETIT, *Electromagnetic theory of gratings*, Springer-Verlag, Berlin, 1980.
- 751 [50] H. R. PHILLIP AND E. A. TAFT, *Kramers-kronig analysis of reflectance data for diamond*,  
752 Phys. Rev., 136 (1964), pp. A1445–A1448.
- 753 [51] N. A. PHILLIPS, *A coordinate system having some special advantages for numerical forecasting*,  
754 Journal of the Atmospheric Sciences, 14 (1957), pp. 184–185.
- 755 [52] H. RAETHER, *Surface plasmons on smooth and rough surfaces and on gratings*, Springer, Berlin,  
756 1988.
- 757 [53] P. J. ROACHE, *Code verification by the method of manufactured solutions*, J. Fluids Eng., 124  
758 (2002), pp. 4–10.
- 759 [54] C. J. ROY, *Review of code and solution verification procedures for computational simulation*,  
760 J. Comp. Phys., 205 (2005), pp. 131–156.
- 761 [55] S. A. SAUTER AND C. SCHWAB, *Boundary element methods*, vol. 39 of Springer Series in Com-  
762 putational Mathematics, Springer-Verlag, Berlin, 2011. Translated and expanded from the  
763 2004 German original.
- 764 [56] J. SHEN AND T. TANG, *Spectral and high-order methods with applications*, vol. 3 of Mathematics  
765 Monograph Series, Science Press Beijing, Beijing, 2006.
- 766 [57] J. SHEN, T. TANG, AND L.-L. WANG, *Spectral methods*, vol. 41 of Springer Series in Computa-  
767 tional Mathematics, Springer, Heidelberg, 2011. Algorithms, analysis and applications.
- 768 [58] J. VIRIEUX AND S. OPERTO, *An overview of full-waveform inversion in exploration geophysics*,  
769 Geophysics, 74 (2009), pp. WCC1–WCC26.